Lab on a Chip

PAPER

View Article Online
View Journal | View Issue

Cite this: *Lab Chip*, 2024, **24**, 5065

Rapid low-cost assembly of modular microvessel-on-a-chip with benchtop xurography†

Shashwat S. Agarwal, ‡[a] Marcos Cortes-Medina,‡[b] Jacob C. Holter, ‡[b] Alex Avendano,[b] Joseph W. Tinapple,[b] Joseph M. Barlage,[c] Miles M. Menyhert,[d] Lotanna M. Onua[d] and Jonathan W. Song *[ae]

Blood and lymphatic vessels in the body are central to molecular and cellular transport, tissue repair, and pathophysiology. Several approaches have been employed for engineering microfabricated blood and lymphatic vessels *in vitro*, yet traditionally these approaches require specialized equipment, facilities, and research training beyond the capabilities of many biomedical laboratories. Here we present xurography as an inexpensive, accessible, and versatile rapid prototyping technique for engineering cylindrical and lumenized microvessels. Using a benchtop xurographer, or a cutting plotter, we fabricated modular multi-layer poly(dimethylsiloxane) (PDMS)-based microphysiological systems (MPS) that house endothelial-lined microvessels approximately 260 μm in diameter embedded within a user-defined 3-D extracellular matrix (ECM). We validated the vascularized MPS (or vessel-on-a-chip) by quantifying changes in blood vessel permeability due to the pro-angiogenic chemokine CXCL12. Moreover, we demonstrated the reconfigurable versatility of this approach by engineering a total of four distinct vessel-ECM arrangements, which were obtained by only minor adjustments to a few steps of the fabrication process. Several of these arrangements, such as ones that incorporate close-ended vessel structures and spatially distinct ECM compartments along the same microvessel, have not been widely achieved with other microfabrication strategies. Therefore, we anticipate that our low-cost and easy-to-implement fabrication approach will facilitate broader adoption of MPS with customizable vascular architectures and ECM components while reducing the turnaround time required for iterative designs.

Received 3rd July 2024,
Accepted 6th October 2024

DOI: 10.1039/d4lc00565a

rsc.li/loc

1. Introduction

The microcirculation contains perfusable networks that are entangled, complex, traditionally difficult to recreate *in vitro*, and whose functionality remains challenging to investigate.[1,2] These challenges have helped propel the use of microsystems engineering techniques, such as micropatterning based on PDMS,[1,3,4] stereolithography,[5,6] extrusion 3-D printing,[7] laser ablation,[8] and machine milling,[9] for reproducing vascular geometry and structures *in vitro*.[10,11] In the context of "vessel-on-a-chip" technology, or vascularized microphysiological systems (MPS), these microsystem engineering techniques all serve the same fabrication goal of encapsulating endothelialized vessels within a platform that can: 1) recreate the complex geometry and function of blood and lymphatic vessels of the microcirculation, 2) allow for biological mechanism study, and 3) enable facile experimental manipulation and analysis.[10,11]

Vessel-on-a-chip systems are recognized as important research tools as they have greatly contributed to advancing our understanding of the role of fluid forces,[4,12] extracellular matrix (ECM) composition,[13] stiffness,[14] and pathological conditions[15] in regulating vascular function. However, the adoption of vessel-on-a-chip systems among biologists and physiologists as well as other researchers with no prior microfabrication training still remains limited.[16] One major constraint is that the established microsystems engineering processes, which underlie the fabrication of MPS, typically require considerable expertise and specialized equipment beyond the reach of many biomedical research labs.[17] For instance, a mainstay for microsystems engineering is patterning micron-scale features using photolithography and

[a] *Department of Mechanical and Aerospace Engineering, The Ohio State University, Columbus, OH 43210, USA. E-mail: song.1069@osu.edu*
[b] *Department of Biomedical Engineering, The Ohio State University, Columbus, OH 43210, USA*
[c] *Department of Biomedical Education and Anatomy, The Ohio State University, Columbus, OH 43210, USA*
[d] *Department of Chemical and Biomolecular Engineering, The Ohio State University, Columbus, OH 43210, USA*
[e] *The Comprehensive Cancer Center, The Ohio State University, Columbus, OH 43210, USA*

† Electronic supplementary information (ESI) available. See DOI: https://doi.org/10.1039/d4lc00565a

‡ Contributed equally.

subsequent PDMS soft lithography of microfluidic devices.[18] However, photolithography requires dedicated cleanroom facilities that are not present or readily accessible at many research institutions. Moreover, PDMS soft lithography produces microchannels that have rectangular cross-sections unlike the circular cross sections or tubular structures that are characteristic of blood or lymphatic vessels *in vivo*. Furthermore, non-circular cross sections are accompanied by inhomogeneous interactions between cells and the adjacent ECM with a non-uniform distribution of shear stress.[19] Several microfabrication techniques such as the combination of needle/rod templating with photolithography, 3D printing, viscous finger patterning and laser ablation have been developed to generate vessels-on-a-chip with cylindrical-based channels encased in an ECM compartment within microfluidic systems.[20–28] Among these, photolithography techniques that use steel needles[29] or PDMS rods[23] to cast open lumens are widely used. After hydrogel polymerization, the rod or needle template is carefully removed using tweezers leaving behind a hollow cylindrical lumen. These lumens are then seeded with endothelial cells to form patent engineered microvessels of a defined diameter such that cell–cell and cell–ECM interactions are homogeneous. Nevertheless, photolithography-enabled fabrication of cylindrical vessels-on-a-chip requires cleanroom facilities and expertise which limits accessibility. Moreover, photolithography of silicon masters includes several complicated and potentially time-consuming steps, including the design and production of photomasks, which slows the turnaround time for design iterations.

Recent advances in commercially available microsystems and rapid prototyping techniques such as 3D printing,[27,30] laser ablation systems,[8,28] and xurography[31] have helped biomedical researchers overcome the complex training and equipment association with traditional microfabrication. Here we focus on xurography, or the use of razor printing using cutting plotters. This technique has increased in popularity as it enables cost-efficient rapid prototyping and assembly of microfluidic devices.[31–33] Typically, xurography involves cutting a polymer sheet with micro-scale precision that is then bonded to other layers or adhesives to form relevant geometries, orientations, and compartmentalization critical for *in vitro* biomimicry of *in vivo* biology and physiology. Importantly, the main capital cost for xurography is a desktop cutting plotter and blades, which can be obtained for less than $1000 and readily deployed on the benchtops of standard wetlabs.[34] As a result, xurography has grown in prominence as a method for fabrication of microfluidic devices due to its simplicity and ability to easily integrate multiple materials.[35] However, the majority of xurography-based microdevices have focused on biochemical applications while cell-culture applications have not yet been extensively demonstrated and characterized, especially 3-D organotypic cultures.[31] To our knowledge, xurography-based fabrication has not been used for engineering vessel-on-a-chip systems with cylindrical microvessels.

In this work, we present xurography as an approach to engineer vascularized MPS containing cylindrical microvessels. We developed and validated our model by quantifying the vascular permeability of the endothelialized lumen in the presence and absence of a pro-angiogenic molecule, CXCL12. We demonstrate the ease and robustness of this modular approach for iterative designs by modifying only a few steps in the fabrication process to generate four different vessel-on-a-chip configurations: 1) single open lumen vessel ("single vessel"), 2) single open lumen vessel perpendicular to a close-ended lumen vessel ("T-shaped vessels"), 3) two opposing close-ended lumen vessels ("opposing vessels"), and 4) single open lumen vessel with multiple distinct ECM regions ("single vessel-multiple ECM regions"). We anticipate that our modular fabrication approach to engineer distinct vessel-on-a-chip configurations with desktop xurography will enable faster and more cost-efficient design iterations of vascularized MPS and increase the adoption of these 3-D culture models in biomedical laboratories.

2. Materials and methods

2.1. Cell culture

Commercially available human umbilical vascular endothelial cells (HUVECs, Lonza) and human dermal lymphatic endothelial cells (HDLECs, PromoCell) were purchased and maintained using endothelial cell growth medium-2 (EGM-2, Lonza, CC-3162) and EGM-2 MV (Lonza, CC-3202), respectively. Cell passage numbers of 5–10 were used in this study. Cells were cultured in a humidified incubator at 37 °C and 5% CO_2 with media exchange every 2 days. Cells were collected for vessel-on-a-chip studies by first washing with 1× Dulbecco's phosphate-buffered saline (PBS) without Mg/Ca (1× DPBS, Gibco, 14190250) followed by detachment using 0.05% Trypsin-EDTA 1× (Gibco, 25300054) for 3–4 minutes to harvest the cells from the T-75 cell culture flasks. After neutralizing trypsin with 10% FBS in DMEM, HUVECs and HDLECs were resuspended in their respective media at a concentration of 10–50 × 10^3 cells per μl in preparation for seeding the lumens of the microfluidic devices.

2.2. Poly(dopamine) coating of PDMS surfaces

Poly(dopamine) (PDA) is a mussel-inspired multifunctional material that has been shown to enhance surface anchorage of ECM hydrogels to PDMS surfaces.[36] To this end, 1 mg ml^{-1} PDA solution was prepared by mixing dopamine hydrochloride (Sigma-Aldrich, H8502) with 10 mM, pH 8.5 tris-HCl buffer (Bioworld, 420204141). To prevent contamination, PDA solution was filtered through a 0.22 μm pore size PES syringe filter. 15 μl of PDA solution was injected in each device through the side gel port – enough to completely fill the gel chamber—and the devices were incubated for 1 hour at room temperature or 37 °C. Subsequently, the PDA solution was aspirated from the ECM chamber followed by rigorously rinsing the ECM chamber with 1× PBS three times. To ensure proper washing, 15 μl of 1× PBS was injected through the side port swishing 10 times *via* pipette.

After washing, the devices were placed in 100 mm culture dishes, wrapped in parafilm, and stored overnight in the incubator at 37 °C.

2.3. Preparation of collagen-based matrices

Polymerized type I collagen (Corning, 354249) matrices were prepared per manufacturer's instructions. Briefly, rat-tail type I collagen (henceforth referred to simply as "collagen") stored in acidic solution was neutralized to pH = 7.4 using sodium hydroxide in 10× phosphate-buffered saline. Sterilized water was then utilized to adjust the final concentration of collagen to 6 mg ml^{-1}. Collagen gels were preincubated at 4 °C for approximately 12 min prior to casting to enhance fiber formation.[37] Upon neutralization and preincubation, collagen gels were pipetted into the ECM region of the microvessel-on-chip system and allowed to polymerize for 30 minutes.

2.4. Microvessel-on-chip assembly using xurography

The assembly for the "single vessel" design of our microvessel-on-a-chip consisted of the following components: i) three 250 μm PDMS layers (Fig. 1A, step 1, part "a"), ii) a single 400 μm PDMS layer (Fig. 1A, step 1, part "b"), iii) a ~260 μm diameter PDMS rod (Fig. 1A, step 9, part "rod"), and iv) a glass slide (Fig. 1A, step 10, part "glass"). This assembly permitted the specification of an inlet and outlet port, a PDMS rod spanning these ports positioned by a razor cut channel, and a central ECM chamber for housing the hydrogel (Video S1†). The 250 μm and 400 μm thick layers (parts "a" and "b", respectively) were formed by spin coating (Specialty Coating Systems, 6812P) uncured PDMS on silanized silicon wafers (University Wafer, 100 mm) at 170 rpm and 115 rpm, respectively. The PDMS-coated wafers were then cured for at least 4 hours in a 65 °C oven. Subsequently, the PDMS layers were peeled off the wafers and cut into rectangular sheets (7.5 × 4 cm) to prepare batch production of devices.

A computer-controlled desktop cutting plotter (Graphtec, CE7000) was used to etch an 8 mm-long and 800 μm-wide rectangular channel in the 400 μm PDMS layer (Fig. 1A, step 2, part "s2") with a plugin for Adobe Illustrator (Graphtec, Cutting Master Version 5). Part "s2" was irreversibly bonded to one of the 250 μm layers (part "a") using plasma oxidation (Harrick Plasma, PDC-32G) to generate the two-layer-thick part "s3" (Fig. 1A, step 3). Note, plasma bonding was aided by spraying 70% ethanol onto the PDMS layers, to facilitate alignment of the layers during device assembly. Next, a second 250 μm layer (part "a") was registered with part "s3", and biopsy punches cored through both parts to create independent parts "a4" and "s4" with aligned inlet and outlet ports: a 1.5 mm punch to make the inlet port, and a 4 mm punch to make the outlet port (Fig. 1A, step 4). With inlet and outlet ports aligned between parts "a4" and "s4", part "a4" was set aside, while part "s4" was used in the subsequent fabrication step. Next, a third part "a" was irreversibly bonded to part "s4" from below with plasma oxidation (Fig. 1A, step 5, part "s5"). Then, a 4 mm biopsy punch cored through part "s5" in between inlet and outlet ports to form the central ECM chamber (Fig. 1A, step 6, part "s6"). Next, the previously set aside part "a4" was plasma bonded to the top of part "s6" to cover the ECM chamber and generate the four-layer assembly (Fig. 1A, step 7, part "s7"). Subsequently, a 1.5 mm biopsy punch was used to core two gel ports on the periphery of the ECM chamber for gel loading (Fig. 1A, step 8, part "s8"). Next, a ~260 μm diameter PDMS rod was inserted into the assembly spanning inlet and outlet ports, guided by the razor cut rectangular microchannel (Fig. 1A, step 9, part "s9"). PDMS rods were created by loading needles (BD, Precision Glide 25G) with uncured PDMS and subsequent curing for at least 30 minutes in a 65 °C oven. The PDMS rods were retrieved by breaking the needles with pliers, pulling with tweezers, and trimming the rod to the desired length. Afterwards, part "s9" was bonded to a glass slide to encapsulate the ECM chamber and for future microscopy (Fig. 1A, step 10, part "s10"). The final device assembly, part "s10", was sterilized with UV light for 30 minutes. While part "s10" can be stored within Petri dishes indefinitely, subsequent steps—polymerization of hydrogel (Fig. 1A, step 11) and rod removal (Fig. 1A, step 12)—were typically performed the day prior to cell seeding.

Prior to adding hydrogel to the device, the ECM chamber was coated with 1 mg ml^{-1} PDA solution, incubated for 1 hour and rinsed thrice with 1× PBS to facilitate gel-PDMS attachment. Subsequently, collagen-based solutions were added in the ECM chamber *via* the gel ports (Fig. 1A, step 11). After collagen gelation, the PDMS rod was removed using tweezers, leaving behind a hollow ductal lumen structure ~260 μm in diameter (Fig. 1A, step 12 and B). Before cell seeding, the lumen was coated with 100 μg ml^{-1} fibronectin for at least 30 minutes and then flushed with cell media. Subsequently, 2 μl of HUVECs suspended at 50 000 cells per μl were seeded into the lumen to form an intact microvessel. The devices were then rotated by placing upside down for 30 minutes, followed by 15-minute intervals on each side, and 20 minutes oriented normally. Afterwards, culture media was added to flush the devices, eliminating any extraneous suspended cells or cellular debris. Media was exchanged daily for all conditions. For devices treated with CXCL12-α, 100 ng ml^{-1} of the chemokine-containing culture media was introduced inside the microvessel 1 day after seeding.

2.5. Microfluidic vessel permeability measurement

Apparent vessel permeability measurements were made on day 3 by passively pumping 20 kDa fluorescein isothiocyanate (FITC)-dextran added to HUVEC culture media (10 μM) into the cell-lined lumen. The change in intensity as the fluorescent dye diffused across the entire vessel lumen was tracked by using time-lapse microscopy. Images were recorded every 5 s for a total of 5 minutes using a Nikon TS-100F microscope equipped with a Q-Imaging QIClick camera controlled with the NIS-Elements software. A custom MATLAB algorithm was then developed to automatically estimate the

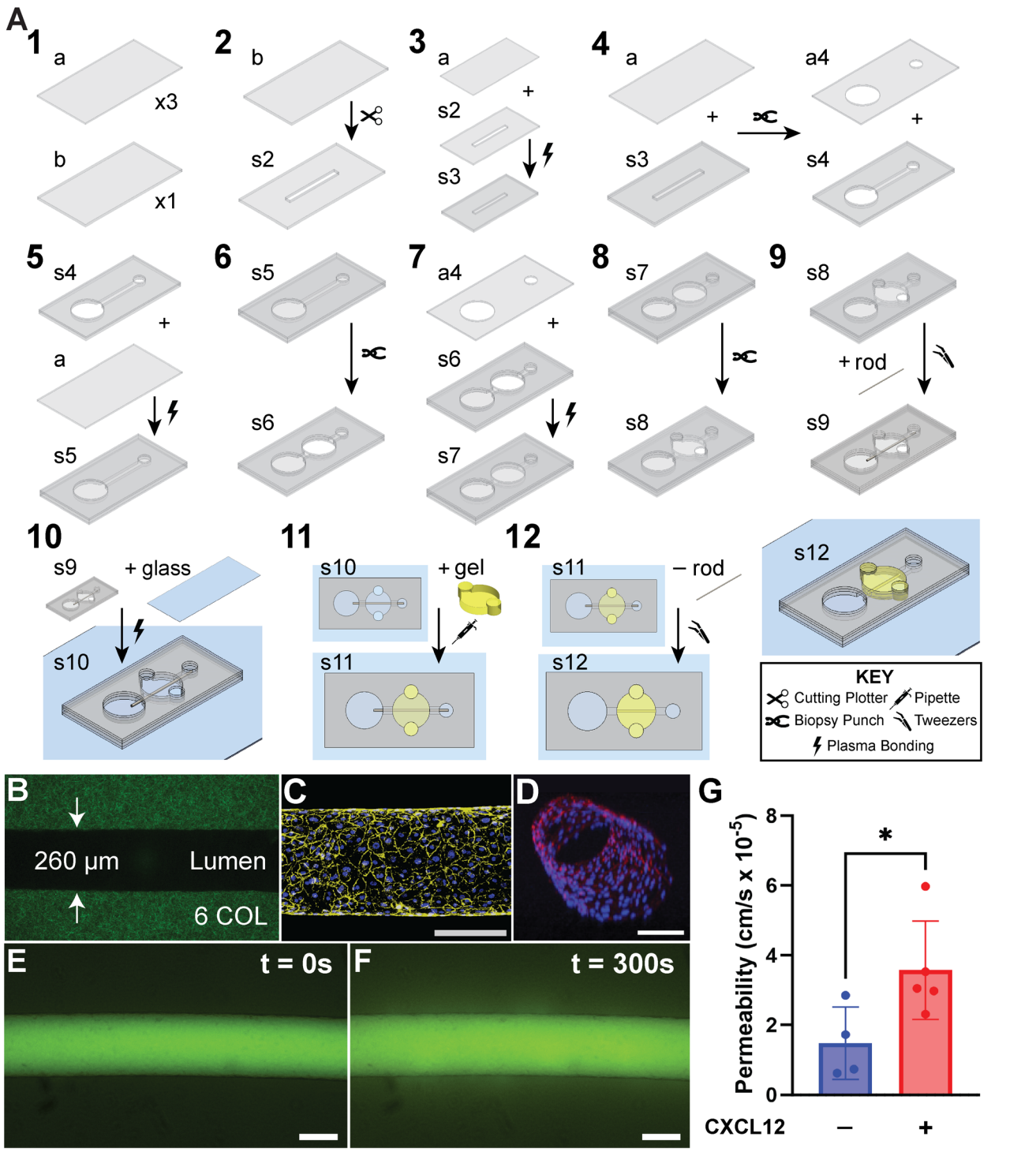

Fig. 1 Engineered cylindrical microvessel model with benchtop xurography. A) Detailed and stepwise fabrication of the open lumen microdevice model. This assembly permits the specification of an inlet and outlet port, a central hydrogel chamber, and a 260 μm PDMS rod that stretches port-to-port across the gel region (Video S1†). B) Confocal reflectance microscopy image of 6 mg ml^{-1} fibrillar type I collagen that is contained within the gel chamber of the model and encases an open lumen structure approximately 260 μm in diameter. C) Confocal *z*-projection of an intact cylindrical microvessel fully lined with HUVECs and stained for adherens junction protein VE-cadherin (monoclonal antibody, yellow) and nuclei counterstain (DAPI, blue). D) 3D render from confocal *z*-stack of cylindrical microvessel stained for F-actin (phalloidin, red) and nuclei (DAPI, blue). E) and F) Changes in fluorescent intensity tracer molecule (20 kDa FITC-conjugated dextran), within the surrounding ECM that has been extravasated from the microvessel was used to calculate apparent vascular permeability after 5 minutes. G) Validation of the functionality of the microvessel by quantifying vessel permeability in the presence and absence of 100 ng ml^{-1} CXCL12-α. CXCL12-α led to an increase in permeability of the HUVEC microvessel. * is p-value < 0.05. Scale bars are 200 μm.

vessel permeability from the time-lapse movies. The script tracks the changes in fluorescent intensity and estimates the vascular permeability by assuming a linear increase in the intensity as the FITC-dextran extravasates to the surrounding ECM by diffusion. Permeability was measured as:

$$P = \frac{1}{I_0} \times \frac{dI}{dt} \times \frac{r}{2},$$

where dI/dt describes the change of intensity as the dye permeates, I_0 equals the instantaneous increase in intensity when the solute is introduced, and r is the radius of the vessel (assuming a cylindrical shape).[38]

2.6. Fluorescence microscopy

We used methods to successfully stain the cells of blood and lymphatic microvessels in collagen hydrogels within our MPS.[39] Briefly, at day 3, cells of microvessels were fixed with 4% paraformaldehyde (PFA) for 30 min at room temperature (RT), permeabilized with 0.2% Triton X-100 for 30 min at RT, blocked with blocking buffer for 30 min at RT, and subsequently stained for either nuclei (DAPI, Sigma-Aldrich, D9542), VE-cadherin (monoclonal antibody, BD Biosciences, 561567), or F-actin (phalloidin, Fisher Scientific, A12379). Microvessels were washed three times between each step with washing buffer: 0.1% Tween 20 in 1× PBS. Blocking Buffer consisted of 1% BSA in washing buffer. VE-cadherin was stained overnight at 4 °C, phalloidin was stained for 60 min at RT, and lastly DAPI was counterstained for 10 min. Images were taken using a Nikon A1R Live Cell Imaging Confocal Microscope controlled with NIS-Elements Software. The same microscope was used for visualization of collagen fibers with confocal reflectance microscopy, which is an imaging modality that requires no staining.[40] We used reflectance microscopy techniques previously described by our group.[41]

2.7. Statistical analysis

Statistical analysis was conducted using Student's *t*-test. Results shown are presented with error bars representing the standard error of the mean (SEM). Each experimental condition was run with at least 4 biological replicates for statistical evaluation. A *p*-value of 0.05 was used as a threshold for statistical significance.

3. Results and discussion

3.1. Xurography enabled fabrication of an endothelialized single open lumen microvessel

Fig. 1A shows detailed or "IKEA-like" assembly instructions for fabricating a single vessel-on-a-chip model, further visualized by Video S1.† We used a PDMS rod of diameter 260 μm to obtain the cylindrical structure, as shown in Fig. 1B. Notably, the entire fabrication process requires a spin-coater, a low-cost benchtop plotter, biopsy punches and a plasma oxidizer, all of which do not require a cleanroom facility. We confirmed the barrier integrity and circular cross-section of the endothelialized microvessel through staining of VE-cadherin and nuclei as shown in Fig. 1C and D. Subsequently, the barrier function of the vessel-on-a-chip model was validated by assessing the extravasation of a fluorescent molecule (20 kDa FITC-dextran) across the vessel wall and into the ECM in the presence and absence of CXCL12, as shown in Fig. 1E and F. The single vessel was subjected to EGM-2 media supplemented with 100 ng ml^{-1} CXCL12 and EGM-2 alone as control for 3 days. CXCL12 exists as several isoforms, is secreted by cancer-associated fibroblasts (CAFs), and is known to stimulate cancer growth and intravasation, as well as regulate vessel permeability through paracrine signaling.[3,42,43] We have also previously shown that CXCL12 mediates blood vessel sprouting and permeability in a microvessel analogue.[3,44] As shown in Fig. 1G, microvessels exposed to the alpha isoform of CXCL12 (CXCL12-α) demonstrated a statistically significant increase in permeability compared to control conditions. While determining vessel responses to CXCL12 is not novel,[3,44] the validation of the assay promotes the feasibility to further interrogate the endothelial lumen with other angiogenic agents, most notably vascular endothelial growth factor (VEGF), or with molecular therapies serving to combat angiogenesis.

3.2. Engineered T-shaped and opposing close-ended vessel configurations

Next, we demonstrated the modularity of our xurography fabricated vessels-on-a-chip technique by incorporating closed or blind ended vessels to the vascular arrangements. Current strategies for templating straight cylindrical vessels typically require the lumen structure to be both continuous and open to both the inlet and outlet. One such example is viscous finger patterning where a continuous tubular lumen structure is formed along a single microchannel by displacing viscous ECM gel with less viscous fluid without needing to insert an external mold.[45] Moreover, several vessel-on-a-chip systems have templated multiple open lumen vessels.[46] These vessels are typically arranged in parallel to each other. However, closed-, or blind-ended vessels are also present in physiological vascular systems. The microanatomy of closed or blind ended vessels are typically attributed to initial lymphatics (or lymphatic capillaries).[47] Yet, closed vessels also occur in the blood microcirculation, such as during wound repair and prior to successful tissue restoration.[48]

A close-ended microvessel was engineered using xurography by modifying the placement of the cylindrical template used in the fabrication process, such that one end of the template is located within the ECM chamber. To achieve this microanatomy, either a PDMS rod or nitinol wire (both ~260 μm in diameter) can be used as a template. Unlike the single open vessel configuration where the cylindrical template can be secured or anchored at two opposing ends (Fig. 1A, step 9), the cylindrical template for a

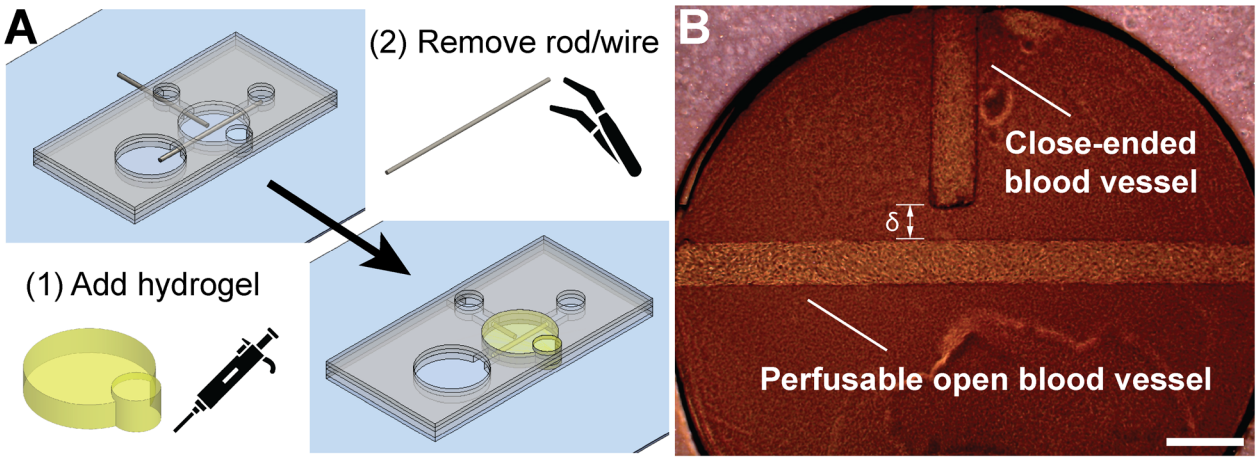

Fig. 2 Engineered close-ended blood vessel oriented perpendicular to a perfusable open blood vessel. A) A PDMS rod and a nitinol wire are inserted from perpendicular directions; the wire is inserted near the center of the ECM chamber to template a terminated blood vessel. B) Phase contrast image of perpendicularly oriented microvessels fully lined with human umbilical vascular endothelial cells (HUVECs). The distance between the closed end of the terminated vessel and the wall of the perfusable vessel (δ) can be specified based on the placement of the rod and wire in A). Scale bar is 500 μm.

close-ended vessel is secured only at one end (Fig. 2A and S1,† step 9). Thus, one of the benefits of using the nitinol wire for a close-ended vessel is that its rigidity facilitates its stable placement as a cylindrical template while the unsecured end is suspended in the ECM gel (Fig. S1,† step 11). Moreover, unlike PDMS rods which need to be recovered manually with tweezers, nitinol wires can be removed post gelation of collagen with a vacuum aspirator.

We fabricated endothelialized "T-shaped vessels" by incorporating an open lumen perpendicular to a close-ended lumen (Fig. 2A). To achieve this configuration, as shown in Fig. S1,† step 2 is modified to cut two perpendicular channels instead of a single channel and a second 1.5 mm biopsy punch is cored in step 4. In addition, a PDMS rod and a nitinol wire were added and removed in steps 9 and 12, respectively, to obtain the microvessels. As shown in Fig. 2B, this vessel-on-a-chip model affords the capability to control the inter-vessel distance (*i.e.*, the distance between the close-ended and the open microvessels, δ). An important design feature due to the xurography fabrication process is that the PDMS rod and nitinol wire are placed on the same layer (step 9 in Fig. S1†). This arrangement ensures that the resultant open vessel and closed vessel of the T-shape are in plane with each other, which is crucial for concurrent imaging of both vessel structures with high resolution 3D imaging (*e.g.*, laser scanning confocal microscopy).

Similarly, we used the close-ended vessel fabrication technique to engineer two opposing close-ended lumen vessels

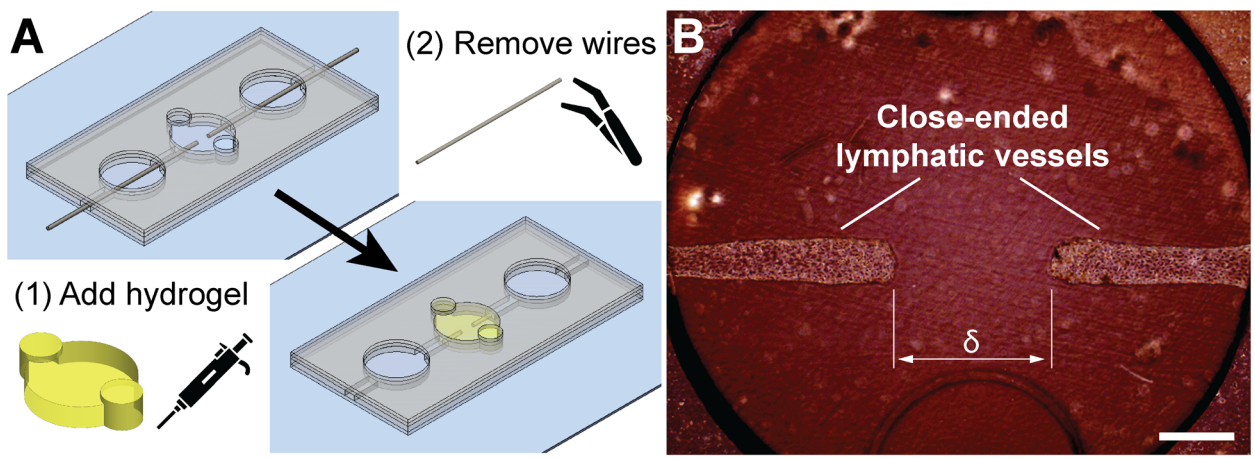

Fig. 3 Two engineered, opposing, close-ended microvessels lined with human dermal lymphatic endothelial cells (HDLECs). A) Two nitinol wires are inserted from opposite ends near the center of the ECM chamber to achieve the cylindrical close-ended structures. After wire removal, the back channel is plugged using liquid PDMS, which is subsequently cured once returned to the 37 °C incubator. B) Phase contrast image of the double close-ended microvessels fully lined with HDLECs. The distance between the closed ends of the vessels (δ) can be specified based on the placement of the wires in A). Scale bar is 500 μm.

as shown in Fig. 3A. To achieve this arrangement, two 260 μm-diameter nitinol wires were added from opposite ports in step 10 of the fabrication process (Fig. S2A†). The rigidity of the nitinol wire affords the capability to control the distance (δ) between the two close-ended lumens, which were seeded with HDLECs. This configuration mimics two opposing blind-ended capillary lymphatics, which can be used to probe vascular dynamics and crosstalk between these structures. Since the two vessels are in the same layer of the multi-layer PDMS device, they are on the same imaging plane and amenable to concurrent imaging with confocal microscopy (Fig. S2B†).

3.3. Engineered single open lumen vessel with multiple distinct ECM regions

In addition to modifying the vascular arrangements, our xurography fabricated microvessel construct is amenable to spatially distinct ECM compartments along the same open vessel lumen (Fig. 4A and B). The "single vessel-multiple ECM regions" configuration models heterogeneous tissue environments by specifying two distinct ECM compositions. One approach for conferring heterogeneous environments along a single microvessel-like structure was shown previously using a multi-layer membrane microdevice.[49] However, one challenge, especially for those without microsystems engineering training, is that membrane microdevices often require several PDMS stamping and bonding steps to ensure proper sealing of layers.[50,51] Moreover, the membranes used for these microdevices are flat, which restricts the endothelia integrated in these microdevices to be planar (*i.e.*, non-circular cross-section). The single vessel-multiple ECM regions arrangement presented here was created by a simple modification to the fabrication of a single open vessel (Fig. 1A). As shown in Fig. S3,† two localized ECM environments were obtained by punching two 2 mm biopsy punches in step 6 rather than using one single 4 mm biopsy punch. Fig. 4B shows two distinct localized ECM chambers containing 3 mg ml^{-1} and 6 mg ml^{-1} collagen embedded with fluorescent microspheres of different colors. The viscosity of the pre-polymerized ECM gel imparts the ability to control the space that is filled by the ECM being injected. Moreover, the sequence of ECM injection plays a crucial role in minimizing overflow of pre-polymerized ECM gel to the neighboring ECM chamber. The 6 mg ml^{-1} collagen pre-polymer was injected first since this gel is denser and more viscous than the 3 mg ml^{-1} collagen (Fig. 4B). This stepwise procedure ensures the formation of a distinct boundary between the two ECM chambers.

The xurography fabrication process also affords the ability to modify the length of the razor cut in step 2 (Fig. S3†). While we show two distinct and localized ECM chambers, we envision that more than two of these chambers can be readily incorporated by extending the length of the microvessel and biopsy punching multiple ECM chambers (Fig. S3,† step 6). Each of these chambers can be used to generate organ- or tissue-specific microenvironments conferred by non-cellular (*e.g.*, ECM proteins) and cellular (*e.g.*, stromal fibroblasts) components encapsulated within the ECM chambers along a single microvessel.[44] Such capabilities would be beneficial to organs-on-a-chip and/or body-on-a-chip studies, which need to mimic ECM environments of several organs on a single MPS. The multiple ECM configuration can also be reconfigured to change the sizes of the ECM chambers and specify the order in which they are serially perfused. Both size and compartmental arrangement have been attributed to be of great importance in organs-on-a-chip systems.[52]

4. Summary and conclusions

Xurography-based approaches have enabled researchers to fabricate microfluidic devices and MPS made from PDMS without the need for cleanroom facilities and lithographic expertise. Thus, xurography has emerged as an attractive and cost-effective rapid prototyping method with pathways for automated batch processing of microdevices.[31] The mechanical

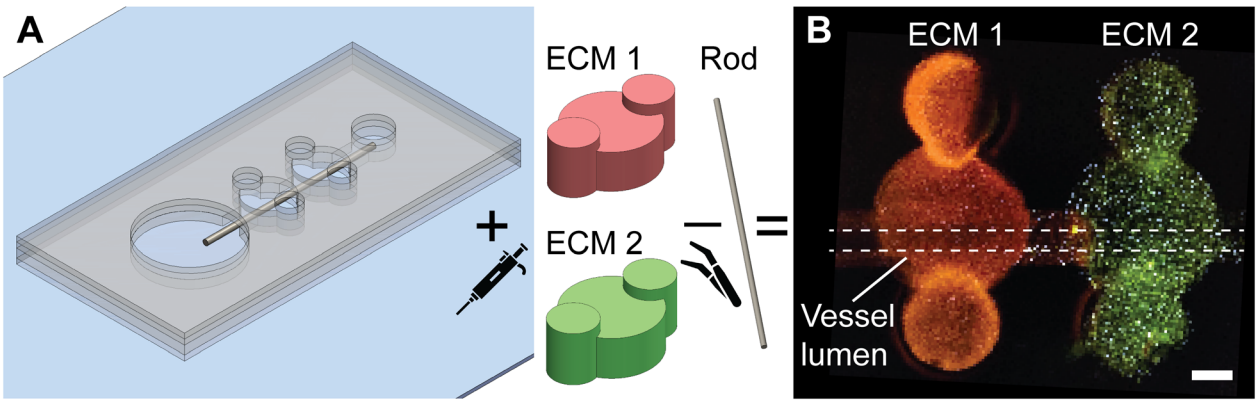

Fig. 4 Engineered single open microvessel exposed to two distinct localized ECM microenvironments. A) The ECM localization is achieved by accommodating two separate central gel chambers and filling them with different hydrogels. After polymerization, the PDMS rod is removed to reveal the single lumen across both ECM compartments, which is then ready for seeding with endothelial cells. B) Fluorescent image of vessel-on-a-chip with distinct ECM environments, which are indicated by incorporating 1 μm fluorescent beads (red or green) prior to casting the two ECM gels. Scale bar is 500 μm.

properties of PDMS are well-suited for cutting plotter machines to pattern and cut distinct geometries for assembly of multi-layer devices. Hence, these devices retain the positive attributes of PDMS, such as optical transparency, biocompatibility, and gas permeability. In this proof-of-concept work, we report a novel implementation of xurography-based fabrication in the engineering of a modular vessel-on-a-chip system. We demonstrate the robustness of the modular approach by fabricating four distinct configurations of the vessel-on-a-chip model, which were obtained by simply modulating one or a few fabrication steps. We believe that these configurations are novel geometries (*e.g.*, T-shaped vessels, opposing close-ended vessels, and single vessel with multiple ECM regions) for the xurography approach.

Our fabrication process enables batch production to increase throughput, with batches consisting of up to 20 devices containing cylindrical microvessels. A typical turnaround time for one batch of 20 devices is ~7 hours prior to the hydrogel step (see Table S1†). This time can be subdivided into "work time" (~2 hours) and "wait time" (~5 hours). In this sense, 20 open lumen devices can be made in approximately 2 hours of labor, which results in a rate of about 6 minutes of labor per device. Furthermore, inter-batch steps can be performed in parallel during wait times to significantly increase throughput. Additionally, total turnaround time can be further optimized: "wait time" can be decreased by increasing the curing temperature and reducing curing time of the spin coated PDMS layers.[53] For instance, Kwak *et al.* reduced the curing time of PDMS from 4 hours to 2 hours by increasing the curing temperature from 65 °C to 80 °C.[54] Alternatively, prefabricated PDMS sheets can be acquired from several commercial vendors worldwide (*e.g.*, SiMPore, DiagnoCine, *etc.*), thereby eliminating the PDMS spin coating step from the workflow.

In addition to showcasing a novel application of xurography and promoting the adoption of vessel-on-a-chip systems for researchers with limited microsystems engineering expertise, we foresee that the xurography-based fabrication techniques presented in this paper will augment current research workflows. During any research project, new questions of interest unfailingly arise, which prompt requests for new microfabricated designs with unique geometries and capabilities. With soft lithography/photolithography-based approaches, a new microfabricated design would require acquisition of a photomask and production of new silicon masters. This process requires many intricate steps with several potential bottlenecks. These bottlenecks may include external factors that are beyond the researcher's control, such as disruptions in reagent supply chains and restricted access to specialized facilities, such as cleanrooms. Both obstacles were heightened to unprecedented levels during the COVID-19 pandemic. Here we replicate a workflow of microvessel designs with increasing complexity, ranging from a single vessel, T-shaped vessels, opposing vessels, and single vessel-multiple ECM regions. Importantly, all the fabrication steps can be conducted in-house within the same laboratory without reliance on external entities or specialized facilities. Thus, while the expected turnaround time for a new microfabricated design using established techniques can be on the order of >1 week, one can realistically expect a new design using xurography-based microfabrication conducted in-house within 1 day.

Physiologically, blood vessel networks expand in a 2-step process that begins with vessel sprouting and is followed by anastomosis, which is a process where sprouts connect to produce a contiguous lumen necessary for new blood flow.[55] Spontaneous anastomosis *in vitro* has been observed in several microfluidic-based models.[39,56–58] The configurations described in the present study may be uniquely positioned for studying certain anastomosis processes that have been observed *in vivo*. For instance, macrophages have been shown to act as chaperones in helping fuse opposing angiogenic sprouts during anastomosis.[59] The opposing vessels configuration may be conducive to study the cellular interactions that underlie this anastomosis process. Also, it has been observed that implanted vascular networks inosculate with the host vessels in a process denoted as "wrapping-and-tapping anastomosis".[60] The engrafted endothelial cells connect to the host vasculature, which diverts blood flow to the developing vessel network. The T-shaped vessels configuration may be amenable for studying the interactions of this anastomosis process. A challenge in observing anastomosis events *in vivo* with real-time microscopy is the requirement to scan an entire vascular plexus while trying to capture dynamic cellular processes. Our model helps address this challenge because of the relative ease of control for geometry of both the lumen and the microdevice due to xurography, which enables the positioning of other cell types (*e.g.*, immune, tumor, or stromal), and inclusion of other factors such as perfusion resulting in tunable shear stress and interstitial flow.[61]

This work also builds upon previous research using templating methods for engineering lumen structures with opportunities to expand this technique. For instance, the PDMS rod templating approach augments the robustness as several PDMS rods can be joined to mimic bifurcated vessel configuration or engineering microvessels with a non-uniform diameter.[23] The latter can be achieved by bonding a higher diameter PDMS rod with a relatively smaller diameter PDMS rod. Furthermore, xurography can also enable microfabrication of parallel vessels by cutting two or more rectangles in the channel layer. Such a configuration has been used to engineer *in vitro* a dense meshwork of perfusable microvessels (~10–25 μm in diameter) formed by vasculogenic self-assembly and flanked by two parallel endothelialized lumens.[58] Moreover, while our studies focused on engineered microvessels, many other tubular structures besides blood and lymphatic vessels exist in physiology, such as mammary ducts and kidney tubules. Several studies have emphasized the importance of 3-D lumen tissue geometry and spatial organization in mediating phenotypic behavior of several cell types,[62–65] such as cancer, endothelial, and kidney epithelial. Thus, our approach for microfabricated microvessels can be readily adapted to study

other tubular structures in physiologic-like environments to further expand the capacity of xurography and broaden its adoption by more researchers.

Data availability

To facilitate access and enhance data sharing, we will use Dryad, which is an open-access repository with both Institutional and Publisher members. Ohio State University is an institutional member of Dryad. Dryad is a generalist repository that meets the U.S. NIH expectations for data sharing.

Conflicts of interest

Jonathan W. Song is a co-founder of and shareholder in EMBioSys, Inc.

Acknowledgements

The authors acknowledge support from an NSF CAREER award (CBET-1752106), the Mark Foundation for Cancer Research (18-024-ASP), the National Heart Lung Blood Institute (R01HL141941), and The Ohio State University Materials Research Seed Grant Program, funded by the Center for Emergent Materials, an NSF-MRSEC, grant DMR-1420451, the Center for Exploration of Novel Complex Materials, and the Institute for Materials Research. Two of the authors (J. C. H. and A. A.) gratefully acknowledge funding from the OSU (Ohio State University) Pelotonia Graduate Fellowship program. Two of the authors (J. C. H. and M. C-M.) thank the support from an NHLBI Graduate Diversity Supplement. One of the authors (M. C-M.) thanks the support from an OSU Graduate Enrichment Fellowship and a Discovery Scholars Fellowship. S. S. A. is funded through the Ohio State University Fellowship and the Ohio State Distinguished University Fellowship. Confocal microscopic images presented in this report were generated using instruments and services at the Campus Microscopy and Imaging Facility (CMIF), The Ohio State University. This facility is supported in part by grant P30 CA016058, National Cancer Institute.

References

1 E. Akbari, G. B. Spychalski and J. W. Song, Microfluidic approaches to the study of angiogenesis and the microcirculation, *Microcirculation*, 2017, **24**(5), DOI: **10.1111/micc.12363**, PubMed PMID: 28182312.

2 S. Kim, H. Lee, M. Chung and N. L. Jeon, Engineering of functional, perfusable 3D microvascular networks on a chip, *Lab Chip*, 2013, **13**(8), 1489–1500, DOI: **10.1039/c3lc41320a**, PubMed PMID: 23440068.

3 C. W. Chang, A. J. Seibel, A. Avendano, M. G. Cortes-Medina and J. W. Song, Distinguishing Specific CXCL12 Isoforms on Their Angiogenesis and Vascular Permeability Promoting Properties, *Adv. Healthcare Mater.*, 2020, **9**(4), e1901399, DOI: **10.1002/adhm.201901399**, PubMed PMID: 31944591; PMCID: PMC7033017, Epub 20200115.

4 J. W. Song and L. L. Munn, Fluid forces control endothelial sprouting, *Proc. Natl. Acad. Sci. U. S. A.*, 2011, **108**(37), 15342–15347, DOI: **10.1073/pnas.1105316108**, PubMed PMID: 21876168; PMCID: PMC3174629, Epub 20110829.

5 B. Grigoryan, S. J. Paulsen, D. C. Corbett, D. W. Sazer, C. L. Fortin, A. J. Zaita, P. T. Greenfield, N. J. Calafat, J. P. Gounley, A. H. Ta, F. Johansson, A. Randles, J. E. Rosenkrantz, J. D. Louis-Rosenberg, P. A. Galie, K. R. Stevens and J. S. Miller, Multivascular networks and functional intravascular topologies within biocompatible hydrogels, *Science*, 2019, **364**(6439), 458–464, DOI: **10.1126/science.aav9750**.

6 W. Y. Wang, D. Lin, E. H. Jarman, W. J. Polacheck and B. M. Baker, Functional angiogenesis requires microenvironmental cues balancing endothelial cell migration and proliferation, *Lab Chip*, 2020, **20**(6), 1153–1166, DOI: **10.1039/c9lc01170f**, PubMed PMID: 32100769; PMCID: PMC7328820.

7 P. V. Hauser, H. M. Chang, M. Nishikawa, H. Kimura, N. Yanagawa and M. Hamon, Bioprinting Scaffolds for Vascular Tissues and Tissue Vascularization, *Bioengineering*, 2021, **8**(11), DOI: **10.3390/bioengineering8110178**, PubMed PMID: 34821744; PMCID: PMC8615027, Epub 20211106.

8 A. Enrico, D. Voulgaris, R. Östmans, N. Sundaravadivel, L. Moutaux, A. Cordier, F. Niklaus, A. Herland and G. Stemme, 3D Microvascularized Tissue Models by Laser-Based Cavitation Molding of Collagen, *Adv. Mater.*, 2022, **34**(11), 2109823, DOI: **10.1002/adma.202109823**.

9 D. J. Guckenberger, T. E. De Groot, A. M. Wan, D. J. Beebe and E. W. Young, Micromilling: a method for ultra-rapid prototyping of plastic microfluidic devices, *Lab Chip*, 2015, **15**(11), 2364–2378.

10 S. Fleischer, D. N. Tavakol and G. Vunjak-Novakovic, From Arteries to Capillaries: Approaches to Engineering Human Vasculature, *Adv. Funct. Mater.*, 2020, **30**(37), 1910811, DOI: **10.1002/adfm.201910811**.

11 S. R. Moses, J. J. Adorno, A. F. Palmer and J. W. Song, Vessel-on-a-chip models for studying microvascular physiology, transport, and function in vitro, *Am. J. Physiol.*, 2021, **320**(1), C92–C105, DOI: **10.1152/ajpcell.00355.2020**, PubMed PMID: 33176110.

12 C.-L. E. Helm, M. E. Fleury, A. H. Zisch, F. Boschetti and M. A. Swartz, Synergy between interstitial flow and VEGF directs capillary morphogenesis *in vitro* through a gradient amplification mechanism, *Proc. Natl. Acad. Sci. U. S. A.*, 2005, **102**(44), 15779–15784, DOI: **10.1073/pnas.0503681102**.

13 K. M. Lugo-Cintron, J. M. Ayuso, B. R. White, P. M. Harari, S. M. Ponik, D. J. Beebe, M. M. Gong and M. Virumbrales-Munoz, Matrix density drives 3D organotypic lymphatic vessel activation in a microfluidic model of the breast tumor microenvironment, *Lab Chip*, 2020, **20**(9), 1586–1600, DOI: **10.1039/d0lc00099j**, PubMed PMID: 32297896; PMCID: PMC7330815, Epub 20200416.

14 F. Bordeleau, B. N. Mason, E. M. Lollis, M. Mazzola, M. R. Zanotelli, S. Somasegar, J. P. Califano, C. Montague, D. J. LaValley, J. Huynh, N. Mencia-Trinchant, Y. L. Negrón Abril, D. C. Hassane, L. J. Bonassar, J. T. Butcher, R. S. Weiss and C. A. Reinhart-King, Matrix stiffening promotes a tumor

vasculature phenotype, *Proc. Natl. Acad. Sci. U. S. A.*, 2017, **114**(3), 492–497, DOI: **10.1073/pnas.1613855114**.

15 S. E. Reid, E. J. Kay, L. J. Neilson, A. T. Henze, J. Serneels, E. J. McGhee, S. Dhayade, C. Nixon, J. B. Mackey, A. Santi, K. Swaminathan, D. Athineos, V. Papalazarou, F. Patella, A. Roman-Fernandez, Y. ElMaghloob, J. R. Hernandez-Fernaud, R. H. Adams, S. Ismail, D. M. Bryant, M. Salmeron-Sanchez, L. M. Machesky, L. M. Carlin, K. Blyth, M. Mazzone and S. Zanivan, Tumor matrix stiffness promotes metastatic cancer cell interaction with the endothelium, *EMBO J.*, 2017, **36**(16), 2373–2389, DOI: **10.15252/embj.201694912**, PubMed PMID: 28694244; PMCID: PMC5556271, Epub 20170710.

16 P. Hargrove-Grimes, L. A. Low and D. A. Tagle, Microphysiological Systems: Stakeholder Challenges to Adoption in Drug Development, *Cells Tissues Organs*, 2022, **211**(3), 269–281, DOI: **10.1159/000517422**, PubMed PMID: 34380142; PMCID: PMC8831652, Epub 20210811.

17 M. Mansouri, J. Lam and K. E. Sung, Progress in developing microphysiological systems for biological product assessment, *Lab Chip*, 2024, **24**(5), 1293–1306, DOI: **10.1039/d3lc00876b**, PubMed PMID: 38230512, Epub 20240227.

18 D. Qin, Y. Xia and G. M. Whitesides, Soft lithography for micro- and nanoscale patterning, *Nat. Protoc.*, 2010, **5**(3), 491–502, DOI: **10.1038/nprot.2009.234**, PubMed PMID: 20203666, Epub 20100218.

19 Q. Vo, K. A. Carlson, P. M. Chiknas, C. N. Brocker, L. DaSilva, E. Clark, S. K. Park, A. S. Ajiboye, E. M. Wier and K. H. Benam, On-Chip Reconstitution of Uniformly Shear-Sensing 3D Matrix-Embedded Multicellular Blood Microvessel, *Adv. Funct. Mater.*, 2024, **34**(10), 2304630, DOI: **10.1002/adfm.202304630**.

20 V. L. Silvestri, E. Henriet, R. M. Linville, A. D. Wong, P. C. Searson and A. J. Ewald, A Tissue-Engineered 3D Microvessel Model Reveals the Dynamics of Mosaic Vessel Formation in Breast Cancer, *Cancer Res.*, 2020, **80**(19), 4288–4301, DOI: **10.1158/0008-5472.Can-19-1564**.

21 P. P. Partyka, G. A. Godsey, J. R. Galie, M. C. Kosciuk, N. K. Acharya, R. G. Nagele and P. A. Galie, Mechanical stress regulates transport in a compliant 3D model of the blood-brain barrier, *Biomaterials*, 2017, **115**, 30–39, DOI: **10.1016/j.biomaterials.2016.11.012**.

22 N. Bouhrira, B. J. DeOre, D. W. Sazer, Z. Chiaradia, J. S. Miller and P. A. Galie, Disturbed flow disrupts the blood-brain barrier in a 3D bifurcation model, *Biofabrication*, 2020, **12**(2), 025020, DOI: **10.1088/1758-5090/ab5898**.

23 J. A. Jiménez-Torres, S. L. Peery, K. E. Sung and D. J. Beebe, LumeNEXT: A Practical Method to Pattern Luminal Structures in ECM Gels, *Adv. Healthcare Mater.*, 2016, **5**(2), 198–204, DOI: **10.1002/adhm.201500608**.

24 L. Yan, C. W. Dwiggins, U. Gupta and K. M. Stroka, A Rapid-Patterning 3D Vessel-on-Chip for Imaging and Quantitatively Analyzing Cell-Cell Junction Phenotypes, *Bioengineering*, 2023, **10**(9), DOI: **10.3390/bioengineering10091080**, PubMed PMID: 37760182; PMCID: PMC10525190, Epub 20230913.

25 C. A. Dessalles, C. Ramón-Lozano, A. Babataheri and A. I. Barakat, Luminal flow actuation generates coupled shear and strain in a microvessel-on-chip, *Biofabrication*, 2021, **14**(1), 015003.

26 A. Herland, A. D. van der Meer, E. A. FitzGerald, T.-E. Park, J. J. Sleeboom and D. E. Ingber, Distinct contributions of astrocytes and pericytes to neuroinflammation identified in a 3D human blood-brain barrier on a chip, *PLoS One*, 2016, **11**(3), e0150360.

27 J. S. Miller, K. R. Stevens, M. T. Yang, B. M. Baker, D.-H. T. Nguyen, D. M. Cohen, E. Toro, A. A. Chen, P. A. Galie, X. Yu, R. Chaturvedi, S. N. Bhatia and C. S. Chen, Rapid casting of patterned vascular networks for perfusable engineered three-dimensional tissues, *Nat. Mater.*, 2012, **11**(9), 768–774, DOI: **10.1038/nmat3357**.

28 C. K. Arakawa, B. A. Badeau, Y. Zheng and C. A. DeForest, Multicellular Vascularized Engineered Tissues through User-Programmable Biomaterial Photodegradation, *Adv. Mater.*, 2017, **29**(37), 1703156, DOI: **10.1002/adma.201703156**.

29 K. M. Chrobak, D. R. Potter and J. Tien, Formation of perfused, functional microvascular tubes in vitro, *Microvasc. Res.*, 2006, **71**(3), 185–196, DOI: **10.1016/j.mvr.2006.02.005**.

30 F. Cantoni, L. Barbe, H. Pohlit and M. Tenje, A Perfusable Multi-Hydrogel Vasculature On-Chip Engineered by 2-Photon 3D Printing and Scaffold Molding to Improve Microfabrication Fidelity in Hydrogels, *Adv. Mater. Technol.*, 2024, **9**(4), 2300718, DOI: **10.1002/admt.202300718**.

31 L. E. Stallcop, Y. R. Alvarez-Garcia, A. M. Reyes-Ramos, K. P. Ramos-Cruz, M. M. Morgan, Y. Shi, L. Li, D. J. Beebe, M. Domenech and J. W. Warrick, Razor-printed sticker microdevices for cell-based applications, *Lab Chip*, 2018, **18**(3), 451–462, DOI: **10.1039/c7lc00724h**, PubMed PMID: 29318250; PMCID: PMC5821501.

32 J. Liu, J. B. Mahony and P. R. Selvaganapathy, Low-cost and versatile integration of microwire electrodes and optical waveguides into silicone elastomeric devices using modified xurographic methods, *Microsyst. Nanoeng.*, 2017, **3**(1), 17040, DOI: **10.1038/micronano.2017.40**.

33 R. Tran, C. A. Hoesli and C. Moraes, Accessible dynamic micropatterns in monolayer cultures via modified desktop xurography, *Biofabrication*, 2021, **13**(2), 025003, DOI: **10.1088/1758-5090/abce0b**.

34 J. I. Martinez-Lopez, M. Mojica, C. A. Rodriguez and H. R. Siller, Xurography as a Rapid Fabrication Alternative for Point-of-Care Devices: Assessment of Passive Micromixers, *Sensors*, 2016, **16**(5), DOI: **10.3390/s16050705**, PubMed PMID: 27196904; PMCID: PMC4883396, Epub 20160516.

35 S. Shahriari, V. Patel and P. R. Selvaganapathy, Xurography as a tool for fabrication of microfluidic devices, *J. Micromech. Microeng.*, 2023, **33**(8), 083002, DOI: **10.1088/1361-6439/ace05d**.

36 S. E. Park, A. Georgescu, J. M. Oh, K. W. Kwon and D. Huh, Polydopamine-Based Interfacial Engineering of Extracellular Matrix Hydrogels for the Construction and Long-Term Maintenance of Living Three-Dimensional Tissues, *ACS Appl. Mater. Interfaces*, 2019, **11**(27), 23919–23925, DOI: **10.1021/acsami.9b07912**.

37 A. Avendano, J. J. Chang, M. G. Cortes-Medina, A. J. Seibel, B. R. Admasu, C. M. Boutelle, A. R. Bushman, A. A. Garg,

C. M. DeShetler, S. L. Cole and J. W. Song, Integrated Biophysical Characterization of Fibrillar Collagen-Based Hydrogels, *ACS Biomater. Sci. Eng.*, 2020, **6**(3), 1408–1417, DOI: **10.1021/acsbiomaterials.9b01873**, PubMed PMID: 32292818; PMCID: PMC7156078, Epub 20200205.

38 V. H. Huxley, F. E. Curry and R. H. Adamson, Quantitative fluorescence microscopy on single capillaries: alpha-lactalbumin transport, *Am. J. Physiol.*, 1987, **252**(1), H188–H197, DOI: **10.1152/ajpheart.1987.252.1.H188**.

39 J. W. Song, D. Bazou and L. L. Munn, Anastomosis of endothelial sprouts forms new vessels in a tissue analogue of angiogenesis, *Integr. Biol.*, 2012, **4**(8), 857–862, DOI: **10.1039/c2ib20061a**, PubMed PMID: 22673771, PMCID: PMC3759296, Epub 20120606.

40 A. O. Brightman, B. P. Rajwa, J. E. Sturgis, M. E. McCallister, J. P. Robinson and S. L. Voytik-Harbin, Time-lapse confocal reflection microscopy of collagen fibrillogenesis and extracellular matrix assembly in vitro, *Biopolymers*, 2000, **54**(3), 222–234, DOI: **10.1002/1097-0282(200009)54:3<222::AID-BIP80>3.0.CO;2-K**, PubMed PMID: 10861383.

41 M. Cortes-Medina, A. R. Bushman, P. E. Beshay, J. J. Adorno, M. M. Menyhert, R. M. Hildebrand, S. S. Agarwal, A. Avendano, A. K. Friedman and J. W. Song, Chondroitin sulfate, dermatan sulfate, and hyaluronic acid differentially modify the biophysical properties of collagen-based hydrogels, *Acta Biomater.*, 2024, **174**, 116–126, DOI: **10.1016/j.actbio.2023.12.018**.

42 D. K. Ahirwar, M. W. Nasser, M. M. Ouseph, M. Elbaz, M. C. Cuitino, R. D. Kladney, S. Varikuti, K. Kaul, A. R. Satoskar, B. Ramaswamy, X. Zhang, M. C. Ostrowski, G. Leone and R. K. Ganju, Fibroblast-derived CXCL12 promotes breast cancer metastasis by facilitating tumor cell intravasation, *Oncogene*, 2018, **37**(32), 4428–4442, DOI: **10.1038/s41388-018-0263-7**, PubMed PMID: 29720724; PMCID: PMC7063845, Epub 20180503.

43 S. Zhao, S. L. Chang, J. J. Linderman, F. Y. Feng and G. D. Luker, A Comprehensive Analysis of CXCL12 Isoforms in Breast Cancer(1,2), *Transl. Oncol.*, 2014, **7**(3), 429–438, DOI: **10.1016/j.tranon.2014.04.001**, PubMed PMID: 24836649; PMCID: PMC4145355, Epub 20140513.

44 J. C. Holter, C. W. Chang, A. Avendano, A. A. Garg, A. K. Verma, M. Charan, D. K. Ahirwar, R. K. Ganju and J. W. Song, Fibroblast-derived CXCL12 increases vascular permeability in a 3-D microfluidic model independent of extracellular matrix contractility, *Front. Bioeng. Biotechnol.*, 2022, **10**, 888431, DOI: **10.3389/fbioe.2022.888431**, PubMed PMID: 36118583, PMCID: PMC9478647, Epub 20220902.

45 L. L. Bischel, S. H. Lee and D. J. Beebe, A practical method for patterning lumens through ECM hydrogels via viscous finger patterning, *J. Lab. Autom.*, 2012, **17**(2), 96–103, DOI: **10.1177/2211068211426694**, PubMed PMID: 22357560; PMCID, PMC3397721, Epub 20120124.

46 N. Zhao, A. F. Pessell, N. Zhu and P. C. Searson, Tissue-Engineered Microvessels: A Review of Current Engineering Strategies and Applications, *Adv. Healthcare Mater.*, 2024, 2303419, DOI: **10.1002/adhm.202303419**.

47 G. W. Schmid-Schonbein, Microlymphatics and lymph flow, *Physiol. Rev.*, 1990, **70**(4), 987–1028, DOI: **10.1152/physrev.1990.70.4.987**.

48 R. S. Sweat, P. C. Stapor and W. L. Murfee, Relationships between lymphangiogenesis and angiogenesis during inflammation in rat mesentery microvascular networks, *Lymphatic Res. Biol.*, 2012, **10**(4), 198–207, DOI: **10.1089/lrb.2012.0014**, PubMed PMID: 23240958; PMCID: PMC3525890.

49 J. W. Song, S. P. Cavnar, A. C. Walker, K. E. Luker, M. Gupta, Y. C. Tung, G. D. Luker and S. Takayama, Microfluidic endothelium for studying the intravascular adhesion of metastatic breast cancer cells, *PLoS One*, 2009, **4**(6), e5756, DOI: **10.1371/journal.pone.0005756**, PubMed PMID, 19484126; PMCID: PMC2684591, Epub 20090601.

50 B.-h. Chueh, D. Huh, C. R. Kyrtsos, T. Houssin, N. Futai and S. Takayama, Leakage-Free Bonding of Porous Membranes into Layered Microfluidic Array Systems, *Anal. Chem.*, 2007, **79**(9), 3504–3508, DOI: **10.1021/ac062118p**.

51 D. Huh, H. Fujioka, Y.-C. Tung, N. Futai, R. Paine, 3rd, J. B. Grotberg and S. Takayama, Acoustically detectable cellularlevel lung injury induced by fluid mechanical stresses in microfluidic airway systems, *Proc. Natl. Acad. Sci. U. S. A.*, 2007, **104**(48), 18886–18891, DOI: **10.1073/pnas.0610868104**, PubMed PMID: 18006663; PMCID: PMC2141877, Epub 20071115.

52 K. Ronaldson-Bouchard and G. Vunjak-Novakovic, Organs-on-a-Chip: A Fast Track for Engineered Human Tissues in Drug Development, *Cell Stem Cell*, 2018, **22**(3), 310–324, DOI: **10.1016/j.stem.2018.02.011**, PubMed PMID: 29499151, PMCID: PMC5837068.

53 N. C. Speller, G. G. Morbioli, M. E. Cato, T. P. Cantrell, E. M. Leydon, B. E. Schmidt and A. M. Stockton, Cutting edge microfluidics: Xurography and a microwave, *Sens. Actuators, B*, 2019, **291**, 250–256, DOI: **10.1016/j.snb.2019.04.004**.

54 T. J. Kwak and E. Lee, In vitro modeling of solid tumor interactions with perfused blood vessels, *Sci. Rep.*, 2020, **10**(1), 20142, DOI: **10.1038/s41598-020-77180-1**.

55 P. Carmeliet and R. K. Jain, Molecular mechanisms and clinical applications of angiogenesis, *Nature*, 2011, **473**(7347), 298–307, DOI: **10.1038/nature10144**.

56 J. H. Yeon, H. R. Ryu, M. Chung, Q. P. Hu and N. L. Jeon, In vitro formation and characterization of a perfusable three-dimensional tubular capillary network in microfluidic devices, *Lab Chip*, 2012, **12**(16), 2815–2822, DOI: **10.1039/C2LC40131B**.

57 X. Wang, D. T. T. Phan, A. Sobrino, S. C. George, C. C. W. Hughes and A. P. Lee, Engineering anastomosis between living capillary networks and endothelial cell-lined microfluidic channels, *Lab Chip*, 2016, **16**(2), 282–290, DOI: **10.1039/C5LC01050K**.

58 J. Paek, S. E. Park, Q. Lu, K.-T. Park, M. Cho, J. M. Oh, K. W. Kwon, Y.-s. Yi, J. W. Song, H. I. Edelstein, J. Ishibashi, W. Yang, J. W. Myerson, R. Y. Kiseleva, P. Aprelev, E. D. Hood, D. Stambolian, P. Seale, V. R. Muzykantov and D. Huh, Microphysiological Engineering of Self-Assembled and

Perfusable Microvascular Beds for the Production of Vascularized Three-Dimensional Human Microtissues, *ACS Nano*, 2019, **13**(7), 7627–7643, DOI: **10.1021/acsnano.9b00686**.

59 A. Fantin, J. M. Vieira, G. Gestri, L. Denti, Q. Schwarz, S. Prykhozhij, F. Peri, S. W. Wilson and C. Ruhrberg, Tissue macrophages act as cellular chaperones for vascular anastomosis downstream of VEGF-mediated endothelial tip cell induction, *Blood*, 2010, **116**(5), 829–840, DOI: **10.1182/blood-2009-12-257832**.

60 G. Cheng, S. Liao, H. Kit Wong, D. A. Lacorre, E. di Tomaso, P. Au, D. Fukumura, R. K. Jain and L. L. Munn, Engineered blood vessel networks connect to host vasculature via wrapping-and-tapping anastomosis, *Blood*, 2011, **118**(17), 4740–4749, DOI: **10.1182/blood-2011-02-338426**.

61 E. W. K. Young, Cells, tissues, and organs on chips: challenges and opportunities for the cancer tumor microenvironment, *Integr. Biol.*, 2013, **5**(9), 1096–1109, DOI: **10.1039/C3IB40076J**.

62 S. G. Rayner, K. T. Phong, J. Xue, D. Lih, S. J. Shankland, E. J. Kelly, J. Himmelfarb and Y. Zheng, Reconstructing the Human Renal Vascular–Tubular Unit In Vitro, *Adv. Healthcare Mater.*, 2018, **7**(23), 1801120, DOI: **10.1002/adhm.201801120**.

63 M. Virumbrales-Munoz, J. M. Ayuso, M. M. Gong, M. Humayun, M. K. Livingston, K. M. Lugo-Cintron, P. McMinn, Y. R. Alvarez-Garcia and D. J. Beebe, Microfluidic lumen-based systems for advancing tubular organ modeling, *Chem. Soc. Rev.*, 2020, **49**(17), 6402–6442, DOI: **10.1039/d0cs00705f**, PubMed PMID: 32760967; PMCID: PMC7521761.

64 J. Tien, U. Ghani, Y. W. Dance, A. J. Seibel, M. C. Karakan, K. L. Ekinci and C. M. Nelson, Matrix Pore Size Governs Escape of Human Breast Cancer Cells from a Microtumor to an Empty Cavity, *iScience*, 2020, **23**(11), 101673, DOI: **10.1016/j.isci.2020.101673**, PubMed PMID: 33163933; PMCID: PMC7599434, Epub 20201014.

65 M. L. Tan, N. Jenkins-Johnston, S. Huang, B. Schutrum, S. Vadhin, A. Adhikari, R. M. Williams, W. R. Zipfel, J. Lammerding, J. D. Varner and C. Fischbach, Endothelial cells metabolically regulate breast cancer invasion toward a microvessel, *APL Bioeng.*, 2023, **7**(4), DOI: **10.1063/5.0171109**.